

A detailed study of the high-mass clump interacting with the bubble N10

Yingxiu Ma^{1,2} • Jianjun Zhou^{1,3} •
Jarken. Esimbek^{1,3} • Weiguang Ji^{1,3} •
Gang Wu^{1,3} • Ye Yuan^{1,2}

© Springer-Verlag ●●●●

Abstract We performed a detailed study of the high-mass clump interacting with bubble N10 based on the spectral lines $^{12}\text{CO}(3-2)$, $\text{HCO}^+(4-3)$, $\text{N}_2\text{H}^+(4-3)$ and $\text{CH}_3\text{OH}(7(0,7)-6(0,6))$ and continuum emission data at 450 μm and 850 μm released on CADC and Spitzer data. Blue-shifted optically thick line $^{12}\text{CO}(3-2)$ seems to indicate that the outer envelope of the high-mass clump is still falling toward the center. Detection of $\text{CH}_3\text{OH}(7(0,7)-6(0,6))$ suggests that a hot core has formed around YSO N10-7. And position-velocity diagram of $\text{N}_2\text{H}^+(4-3)$ indicates the cold dense core of the clump has not been destroyed by the star formation activities. The mass of N10-7 is about $27.44 M_\odot$. The ratio $\text{HCO}^+(4-3)/\text{N}_2\text{H}^+(4-3)$ in the outer part of the clump is larger than that in the inner part of it. The reason may be that the CO abundance relative to $\text{N}_2\text{H}^+(4-3)$ increased in the outer part of the high-mass clump, more $\text{N}_2\text{H}^+(4-3)$ were converted into $\text{HCO}^+(4-3)$.

Keywords HII regions – ISM; clouds – stars; formation

Yingxiu Ma
Jianjun Zhou
Jarken. Esimbek
Weiguang Ji
Gang Wu
Ye Yuan

¹Xinjiang Astronomical Observatory, Chinese Academy of Sciences, Urumqi 830011, PR China

²University of Chinese Academy of Sciences, Beijing 100080, PR China

³Key Laboratory of Radio Astronomy, Chinese Academy of Sciences, Urumqi 830011, PR China

1 Introduction

The expansion of the HII regions is extreme interest to studies of star formation as their expansion may trigger new generations of star formation into being within the molecular material surrounding the bubbles (Thompson et al. (2012)). Evidence of triggering has been reported by many authors (e.g. Deharveng et al. (2010); Zavagno et al. (2010); Kang et al. (2009)). It should be noted, the majority of observational studies into triggered star formation near SNR or HII regions take a phenomenological approach, the evidence of triggered star formation is not very conclusive (Kendrew et al. (2012)). The statistical approach may address the uncertainties inherent in observations of individual HII regions. One detailed statistical study of massive star formation in the environment of 322 Spitzer mid-infrared bubbles by using the Red MSX source survey for massive young stellar objects (YSOs) suggest that the fraction of massive stars in the Milky Way formed by triggering could be between 14 and 30 per cent (Thompson et al. (2012)). Kendrew et al. (2012) made a similar statistical study with 5106 infrared bubbles, they estimated that approximately 22 per cent of massive young stellar stars may have formed as a result of feedback from expanding HII regions. Therefore, the infrared dust bubbles could be good sites for us to find high-mass YSOs and study the process of high-mass star formation.

N10 is a bright mid-infrared and radio continuum bubble with an elliptical or slight cometary shape with an opening at southeast of bubble (Watson et al. (2008)). Its kinematic distance is about 4.6 kpc (Deharveng et al. (2010)). The bubble is bordered on two sides by infrared dark clouds (IRDCs), they are interacting with the HII regions (Deharveng et al. (2010)). Especially for the IRDC in which one medium-to-high mass YSO has been found by Watson et al. (2008), the YSO

is coincident with one very dense dust core (Miettinen (2012)). So this IRDC is one high-mass clump and is forming YSOs. It provide us a opportunity to study initial conditions and processes of YSO's formation and triggered star formation.

In this paper, we study the high-mass clump and high-mass YSO formed in it based on archive data, which including continuum data at wavelenghtes 1100 μm , 850 μm , 450 μm and molecular lines of $^{12}\text{CO}(3-2)$, $\text{HCO}^+(4-3)$, $\text{N}_2\text{H}^+(4-3)$, $\text{CH}_3\text{OH}(7(0,7)-6(0,6))$. The observational details and data analysis are presented in the following sections.

2 Data

Three large-scale survey results were used in our study, which includes Galactic Legacy Infrared Mid-Plane Survey Extraordinaire (GLIMPSE), the NRAO VLA Sky Survey (NVSS) and BOLOCAM Galactic Plane Survey (BGPS). GLIMPSE is performed using the Spitzer Space Telescope by Spitzer-Infrared Array Camera (IRAC). It is a mid-infrared survey of the inner Galaxy at 3.6, 4.5, 5.8 and 8 μm with angular resolution of between $1''.5$ and $1''.9$, and a very large catalog of stars were extracted from the survey (Churchwell et al. (2009)). Here we used the mosaicked images from GIMPSE acquired by Spitzer-IRAC at 8 μm and the Point-Source catalog. NVSS is a 1.4 GHz radio continuum survey covering the entire sky north of -40 deg declination with an angular resolution of about $45''$ (Condon et al. (1998)). BGPS is a 1.1 mm continuum survey of the Galactic Plane made using Bolocam on the Caltech submillimeter Observatory, the survey coverage totals 170 square degrees (with $33''$ FWHM effective resolution) and detected about 8400 point sources (Rosolowsky et al (2010)).

In addition, we used the James Clerk Maxwell Telescope (JCMT) data released on Canadian Astronomy Data Centre (CADC), they including $^{12}\text{CO}(3-2)$, $\text{HCO}^+(4-3)$, $\text{N}_2\text{H}^+(4-3)$, $\text{CH}_3\text{OH}(7(0,7)-6(0,6))$ data and dust continuum emission at 450 μm and 850 μm . The co-added spectral cubes were binned to 0.2 km s^{-1} , and the data were smoothed with $6''$ Gaussian kernel. The final spatial resolution of each cube is $16''$ (Smith et al. (2008)). The angular resolution of 450 μm and 850 μm is $8''.5$ and $14''.5$ respectively (Leeuw & Robson (2009)).

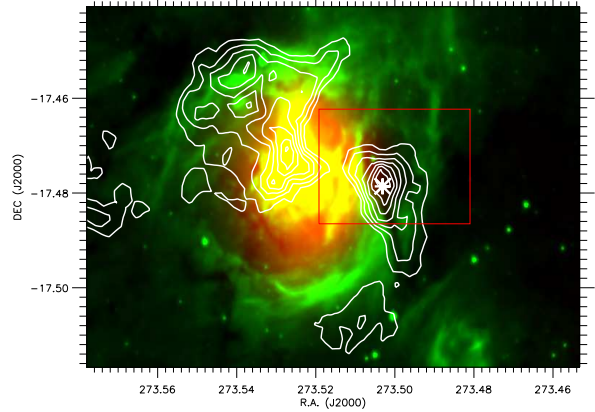


Fig. 1 N10, the $^{12}\text{CO}(3-2)$ contour levels range from 90.0 to 159.5 by 9.93 K km s^{-1} are superimposed on the composite colour image with 20 cm emission in red and 8 μm emission in green. The high-mass clump which we study in detail was marked with one red square. The white star denotes the YSO (N10-7) identified by Watson et al. (2008).

3 Results and discussion

3.1 N10

Figure 1 shows the $^{12}\text{CO}(3-2)$ emission contours over the two colour image with 20 cm emission in red and 8 μm emission in green. The border of N10 is well traced by the 8 μm emission. The 20cm emission in the bubble indicates that there is a large HII region ionized by central stars. The high-mass clump, which we will study in detail, was marked with one red square. An obvious arch border appears between the bubble and the high-mass clump, which suggests that there exists strong interaction. One very compact CO cloud is coincident with the high-mass clump, the medium-to-high-mass YSO (N10-7) identified by Watson et al. (2008) is located at the center of it. The more extended CO cloud appear on the upper left to the center of N10. The CO emission toward the center of the bubble in projection could be arising from the front or back side of the bubble.

We estimated the dynamical age of N10 using the model described by Dyson & Williams (1980) with a given radius R as:

$$t(R) = \frac{4 R_s}{7 c_s} \left[\left(\frac{R}{R_s} \right)^{\frac{7}{4}} - 1 \right] \quad (1)$$

where c_s is the sound velocity in the ionized gas ($c_s = 10 \text{ km s}^{-1}$) and R_s is the radius of the Strömgen sphere given by $R_s = (3 N_{Ly\alpha} / 4\pi n_0^2 \alpha_\beta)^{\frac{1}{3}}$, where $N_{Ly\alpha}$ is the number of ionizing photons emitted by the star per second, n_0 is the original ambient density, and $\alpha_\beta = 2.6 \times 10^{-13} \text{ cm}^3 \text{ s}^{-1}$ is the hydrogen recombination

coefficient to all levels above the ground level. Here we adopt a Lyman continuum photon flux of about $2.2 \times 10^{49} ph s^{-1}$ (Watson et al. (2008)) and a radius of 1.61 pc. For that no CO cores look like swept by expanding HII region on the border of N10, it is difficult for us to estimate the original ambient density of N10. Massive star formations usually take place in the giant molecular clouds and the densities of the giant molecular clouds are about 10^3 to $10^4 cm^{-3}$ (Goldsmith. (1987)). So it seems to be safe for us to assume the low value of original ambient density of N10 is about $10^3 cm^{-3}$ and obtain a lower bound on the dynamical age, about 9.17×10^4 yr. Taking into consider that stars are formed in the dense clumps of the giant molecular cloud, the true original ambient density may be larger than that we assumed, the true dynamical age of N10 should be larger than 9.17×10^4 yr.

3.2 The High-mass Clump

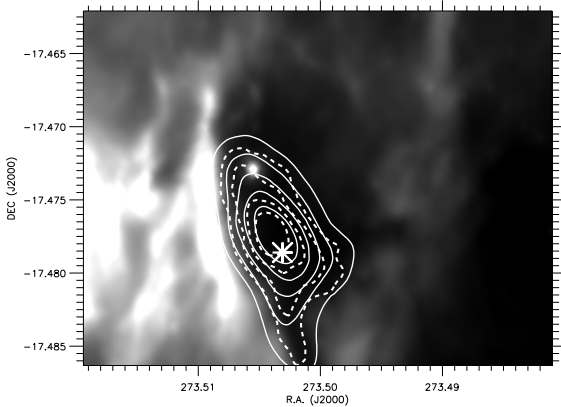


Fig. 2 The white solid contours denote $850 \mu m$ emission, contour levels range from 0.77 to 3.43 by 0.53 Jy / beam. The white dotted contours denote $450 \mu m$, contour levels range from 3.57 to 11.95 by 2.10 Jy / beam. The lowest levels of $850 \mu m$ and $450 \mu m$ are both larger than 3σ . The background is $8 \mu m$ emission. The star represents N10-7.

Past continuum observations at different wavelength have proven that there is one dust condensation in the high-mass clump, the YSO (N10-7) is forming in it (Miettinen (2012)). The JCMT continuum observation results at $450 \mu m$ (white dotted contours) and $850 \mu m$ (white solid contours) display a elongated dust core from north to south (see Fig.2). N10-7 is nearly at the center of it. No mid-IR diffuse emission and lack of 20 cm continuum emission suggest that high-mass star formation is in its very early stage, or the high-mass YSO was embedded in the clump very deeply.

The total dust mass of the clump is calculated using $M = S_\nu D^2 / k_\nu B_\nu(T_d)$, where S_ν is the flux at frequency

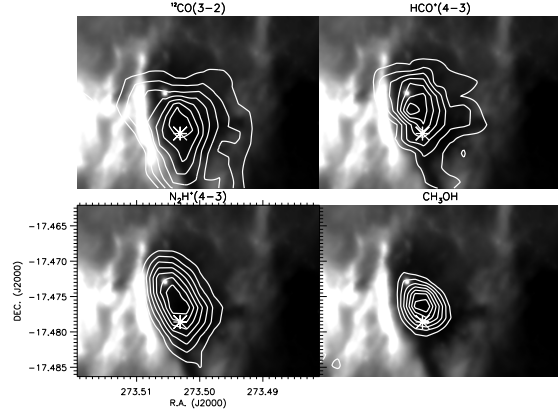


Fig. 3 $^{12}CO(3-2)$, $HCO^+(4-3)$, $N_2H^+(4-3)$ and $CH_3OH(7(0,7) - 6(0,6))$ contours map of the clump are superimposed on the $8 \mu m$ emission. The contour levels range from 90.0 to 159.5 by $9.93 K km s^{-1}$ for $^{12}CO(3-2)$, 3.0 to 15.78 by $1.83 K km s^{-1}$ for HCO^+ , 3.0 to 14.43 by $1.63 K km s^{-1}$ for N_2H^+ and 3.0 to 17.15 by $2.02 K km s^{-1}$ for $CH_3OH(7(0,7) - 6(0,6))$. The star represents N10-7.

ν , D is the distance (4.6 kpc), $B_\nu(T_d)$ is the plank function, and k_ν is the dust opacity per unit gas /dust mass. T_d is the dust temperature, it was obtained by SED fitting with a simple greybody model. The total flux of the clump at $450 \mu m$, $850 \mu m$ and $1.1 mm$ are about 99.33, 13.30 and 7.6 Jy, respectively. The flux at 450 and $850 \mu m$ were derived from JCMT data by ourself, the flux at $1.1 mm$ were obtained from BGPS point source catalog and multiplied by a factor of 1.5. The best fitted result indicates that $T_d = 27 K$. Using the dust opacity of $k_{850} = 0.02 cm^2 g^{-1}$ obtained from Ossenkopf & Henning (1994), the ratio of dust to gas is taken as 0.01. We derived a total mass of $M = 908 M_\odot$ from $850 \mu m$ flux. The area of the clump is 1333 arcsec square. Assuming the clump is spherical, we get the core radius of $20''.6$ (corresponding to 0.46 pc). Then the average number density is $4.59 \times 10^4 cm^{-3}$. Following Beuther et al. (2012) and Longmore et al. (2012), we assume $\rho \propto r^{-2}$ and calculate Virial mass using the formula of Maclaren, Richardson and Wolfendale (1988).

$$M_{vir} = 126 R \Delta V^2 \quad (2)$$

where ΔV is the full width at half-maximum intensity in kms^{-1} , R is the radius of the molecular cloud in parsecs, M is cloud mass in unit of solar mass. Since star is formed in the cold dense core traced by N_2H^+ , we used the Gaussian line width of N_2H^+ obtained at the position of YSO (N10-7) to calculate the Virial mass of the clump. Finally, we obtained $M_{vir} = 1640 M_\odot$. This indicate the clump may be gravitational stable. However, Miettinen (2012) obtained a total mass of $3335 \pm 704 M_\odot$ for the clump based on $870 \mu m$ observation with Apex submillimeter telescope. The mass

difference may be due to the observation sensitivity difference between the two telescopes. If the result of Miettinen (2012) is true, the clump tends to be gravitationally unstable. Taking into account that the clump is forming one YSO in it, it seems to be more reasonable. Just as that pointed out by Beuther et al. (2012), there are large uncertainties for the mass estimated from the dust continuum emission and Virial mass calculated with N_2H^+ , such a result is not very conclusive.

3.3 The kinematics of the clump

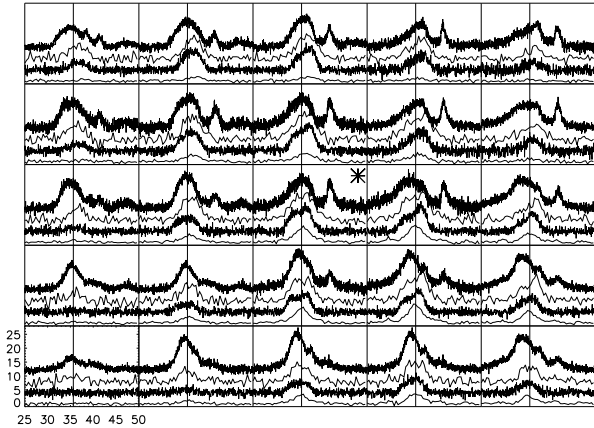


Fig. 4 The molecular profiles extracted from the positions around the YSO N10-7 are plotted, the panel marked by a star corresponds to the YSO N10-7. From up to down in each panel is $^{12}CO(3-2)$, $HCO^+(4-3)$, $N_2H^+(4-3)$, $CH_3OH(7(0,7)-6(0,6))$, respectively. The velocity is between 25 to 50 km/s. CH_3OH , N_2H^+ , HCO^+ profiles are scaled up by a factor 5, 3 and 5, respectively, and their base line is added 4, 8, 12 $K km s^{-1}$, respectively. The vertical line indicates the system velocity of the high-mass clump which is $35.64 km s^{-1}$.

N_2H^+ is not strongly affected by freeze out on grain surfaces, it is a good tracer of younger cold and massive cloud cores. HCO^+ is a highly abundant molecule, with abundance especially enhanced around regions of higher fractional ionization. It is also enhanced by the presence of outflows where shock-generated radiation fields are present (Vasyunina et al. (2011)). CH_3OH molecules are formed in the icy mantles of interstellar dust grains by hydrogenation of CO molecules at temperature of 10K, as the young protostellar object evolves and warms up its environment the CH_3OH molecule sublimates from the dust grains into the gas phase at 100K (Torstensson (2011)). Detection of $HCO^+(4-3)$ and CH_3OH toward the high-mass clump indicates that one hot core has formed around the YSO N10-7. On the other hand, detection of $N_2H^+(4-3)$ indicates star formation in the clump is still in its early

stage, the natal molecular cloud was not destroyed by the feedback of YSO (see Fig.3).

Fig.4 displays the $^{12}CO(3-2)$, $HCO^+(4-3)$, $N_2H^+(4-3)$, $CH_3OH(7(0,7)-6(0,6))$ profiles according to their position around the YSO N10-7. Here $CH_3OH(7(0,7)-6(0,6))$, $N_2H^+(4-3)$ and $HCO^+(4-3)$ profiles are scaled up by a factor of 5, 3 and 5, respectively. The panel marked by a star indicates the position of YSO N10-7. The vertical line in the map indicates the system velocity ($35.64 km s^{-1}$) of the high-mass clump. We noted that the profiles of optically thick line $^{12}CO(3-2)$ include two components at velocity 34.57 and $41.77 km s^{-1}$. The first is the stronger one and is usually blue-shifted with respect to the system velocity. This component traces the high-mass clump, the blue-shifted profiles of it may indicate that the outer envelope traced by CO is still falling toward the center. The profiles of $HCO^+(4-3)$ in the all upper two rows and the left two panels of the third and fourth rows are red-shifted with respect to the system velocity. The $N_2H^+(4-3)$ profile at the position of YSO shows evidence of self-absorption dip. The profiles in upper two rows of panels are red-shifted with respect to the system velocity, while in the lower three rows of panels they become blue-shifted. The position-velocity diagram of $N_2H^+(4-3)$ shows a velocity gradient along the major axis of the high-mass clump (see Fig.5). Such a velocity gradient may be a combination of both rotation and infall motions of the cold dense core (Tobin et al. (2012)). This supports our idea that the cold dense core of the clump has not been destroyed by the feedback of the YSO N10-7 yet. The optically thin $CH_3OH(7(0,7)-6(0,6))$ profiles have only one peak with obvious line wings, but corresponding position-velocity diagram (see Fig.6) displays only slightly red-shifted and blue-shifted lobes. In some extent, this supports the existence of outflow. However, other motions such as rotation, infall and turbulence could also cause this effect, we cannot exclude these motions. More high-resolution observations and studies are needed to draw a conclusive result.

Assuming that line wings of $CH_3OH(7(0,7)-6(0,6))$ indicate outflows truly, we plot the blue and red lobe of the outflow (see Fig.7), the distribution of red lobe is much larger than that of blue lobe. The background is the ratio $HCO^+(4-3)/N_2H^+(4-3)$. It is interesting to find that this ratio $HCO^+(4-3)/N_2H^+(4-3)$ in the outer part is larger than that in the inner part of the clump. For that HCO^+ is created by the reaction between N_2H^+ and CO. The reason may be that the CO abundance relative to $N_2H^+(4-3)$ increased in the outer part of the high-mass clump, more $N_2H^+(4-3)$ were converted into $HCO^+(4-3)$. Increasing of the relative abundance of $HCO^+(4-3)$ increases the ratio

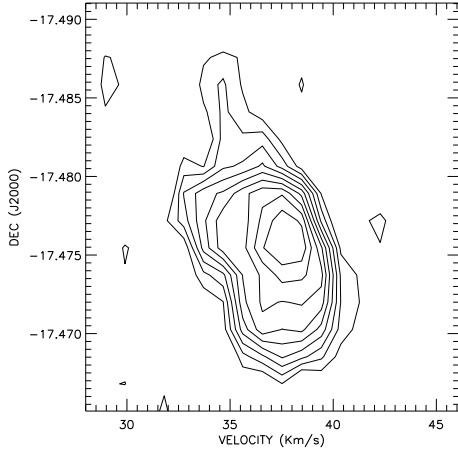


Fig. 5 PV diagram of $N_2H^+(4-3)$ emission along the major axis of the high-mass clump. The contours are from 10% to 90% with steps of 10% of the peak of the integrated intensity.

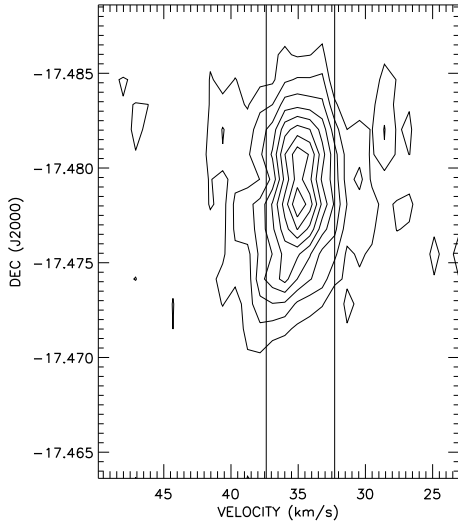


Fig. 6 PV diagram for the $CH_3OH(7(0,7)-6(0,6))$ emission along the major axis of the high-mass clump. The contours are from 10% to 90% with steps of 10% of the peak of the integrated intensity. The vertical black lines indicate the blue- and red-shifted components' velocity boundary.

of $HCO^+(4-3)/N_2H^+(4-3)$. The distribution of $HCO^+(4-3)$ is nearly the same as that of red lobe. This is consistent with the conclusion that $HCO^+(4-3)$ abundance will be enhanced by the presence of outflows. No 20cm continuum emission was detected to the clump suggests that it could not be highly fractional ionized. Enhanced $HCO^+(4-3)$ abundance is likely caused by the outflow. This is also consistent with the fact that most profiles of $HCO^+(4-3)$ are red-shifted with respect to the system velocity.

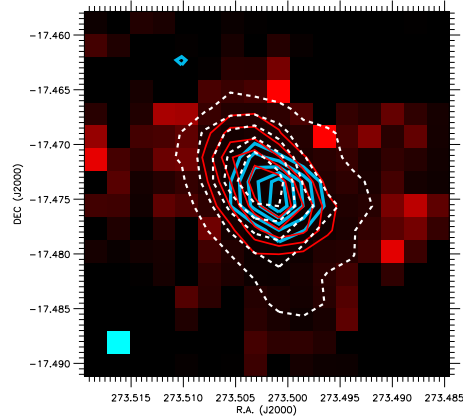


Fig. 7 The components of the CH_3OH outflow superimposed on the integrated intensity ratio $HCO^+(4-3)/N_2H^+(4-3)$ (red background). The velocity components is integrated in $(27,32.5)$ and $(37.4,42.5)$ $km\ s^{-1}$ for its blue and redshifted lobes, the blue and red contours represent blue lobe and red lobe, respectively. The white contours denote $HCO^+(4-3)$ molecule's emission.

3.4 SED fitting of the central massive star

Watson et al. (2008) fitted the SED of the young stellar object (N10-7) formed in the high-mass clump using the tool developed by Robitaille et al. (2006) based on the Spitzer IRAC data, they found that N10-7 is one Stage I YSO with a mass of $12.4 M_\odot$. However, their SED fitting results may not be very accurate due to the lack of data at longer wavelengths. We fit the SED of N10-7 using more data, which including Spitzer-IRAC data at 3.6, 4.5, 5.8 and 8 μm , SCUBA data at 450 and 850 μm and BOLOCAM data at 1.1 mm. The visual extinction is estimated from the classical relations $N_{H+H_2}/E(B-V) = 5.8 \times 10^{21} particles\ cm^{-2}\ mag^{-1}$ (Bohlin et al. (1978)) and $A_v = 3.1E(B-V)$, so we obtain $A_v = 5.34 \times 10^{-22} N_{H_2}$. According to Shetty et al. (2011) and Ji et al. (2012), we used the X factor between H_2 and ^{12}CO to estimate the column density of the clump. So $N_{H_2} = X \times W_{CO}[cm^{-2}]$, where W_{CO} is the integrated ^{12}CO intensity, $W_{CO} = \int T_{mb} dv\ cm^{-2}\ K\ km\ s^{-1}$. Finally we obtained the A_v is between 5 to 30 mag.

We selected the best SED fitting model (see Fig.8). The source age is $1.81 \times 10^4 yr$, the source mass is $M_\star = 27.44 M_\odot$, the disk mass $M_{disk} = 4.52 \times 10^{-2} M_\odot$, the envelope mass $M_{env} = 1.48 \times 10^3 M_\odot$, and the envelope accretion rate $\dot{M}_{env} = 3.34 \times 10^{-3} M_\odot/yr$. N10-7 satisfy the criteria $\dot{M}_{env}/M_\star > 10^{-6} yr^{-1}$ (Robitaille et al. (2007)), and is one stage I YSO.

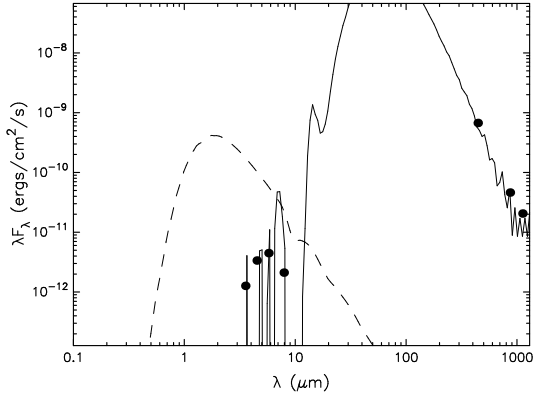


Fig. 8 The SED fitting of high-mass YSO N10-7. Black line shows the best fit. The dashed line shows the stellar photosphere corresponding to the central source of the best fitting model, as it would look in the absence of circumstellar dust. The black points represent the input data at 3.6, 4.5, 5.8, 8, 450, 850 and 1100 μm .

4 Summary

We studied the high-mass clump associated with the bubble N10 in detail based on the Spitzer data, continuum observations at 450, 850 and 1100 μm and spectral lines of $^{12}CO(3-2)$, $HCO^+(4-3)$, $N_2H^+(4-3)$ and $CH_3OH(7(0,7)-6(0,6))$.

We draw some tentative results for the high-mass clump. Optically thick line $^{12}CO(3-2)$ are all blue-shifted with respect to the system velocity, this seems to indicate that the outer envelope of the high-mass clump is still falling toward the center. The position-velocity diagram of $N_2H^+(4-3)$ indicates the cold dense core of the clump has not been destroyed by the star formation activities in it. Detection of $CH_3OH(7(0,7)-6(0,6))$ suggests that a hot core has formed due to the feedback of YSO N10-7. The mass of N10-7 is about $27.44 M_\odot$. The line wings of $CH_3OH(7(0,7)-6(0,6))$ seems to trace the outflow excited by N10-7. The ratio $HCO^+(4-3)/N_2H^+(4-3)$ in the outer part of the clump is larger than that in the inner part of it. The reason may be that the CO abundance relative to $N_2H^+(4-3)$ increased in the outer part of the high-mass clump, more $N_2H^+(4-3)$ were converted into $HCO^+(4-3)$.

Acknowledgements This work was funded by The National Natural Science Foundation of China under grant 10778703, and partly supported by China Ministry of Science and Technology under State Key Development Program for Basic Research (2012CB821800) and The National Natural Science Foundation of China under grant 10873025.

References

- Beuther, H., Tackenberg, J., Linz, H. et al. 2012, A&A, 538A, 11
- Bohlin, R. C., Savage, B. D., & Drake, J. F. 1978, ApJ, 224, 132
- Churchwell, E., Babler, B. L., & Meade, M. R., et al. 2009, PASP, 121, 213C
- Condon, J. J., Cotton, W. D., & Greisen, E. W., et al. 1998, AJ, 115, 1693
- Deharveng, L., Schuller, F., & Anderson, L. D., et al. 2010, A&A, 523A, 6
- Dyson, J. E., & Williams, D. A. 1980, Physics of the interstellar medium (New York: Halsted Press), 204
- Goldsmith, P. F., 1987, ASSL, 134, 51
- Ji, W. G., Zhou, J. J., Esimbek, J., et al. 2012, A&A, 544A, 39
- Kang, M., Bieging, J. H., Kulesa, C. A., et al. 2009, APJ, 454, 463
- Kendrew, S., Simpson, R., Bressert, E., et al. 2012, APJ, 755, 71K
- Leeuw, L. L., & Robson, E. I. 2009, APJ, 517, 527
- Longmore, S. N., Rathborne, J., Bastian, N., et al. 2012, ApJ, 746, 117
- Maclaren, I., Richardson, K. M., & Wolfendale, A. M. 1988, ApJ, 333, 821
- Miettinen, O. 2012 A&A, 542A,101
- Ossenkopf, V., & Henning, T. 1994, A&A, 291, 943
- Robitaille, T. P., Whitney, B. A., Indebetouw, R., et al. 2006, ApJS, 167, 256
- Robitaille, T. P., Whitney, B. A., & Indebetouw, R., et al. 2007, ApJS, 169, 328
- Rosolowsky, E., Dunham, M. K., Ginsburg, A., et al. 2010, APJS, 188, 123R
- Shetty, R., Glover, S. C., Dullemond, C. P., et al. 2011, MNRAS, 412, 1686
- Smith, H., et al. 2008, Proc. SPIE, 7020, 70200Z1
- Thompson, M. A., Urquhart, J. S., Moore, T. J. T., et al. 2012, MNRAS, 421, 408
- Tobin, J. J., Hartmann, L., Bergin, E., et al. 2012, ApJ, 748, 16
- Torstensson, K. J. E. 2011, Ph. D. thesis
- Vasyunina, T., Linz, H., Henning, Th., et al. 2011, A&A, 527A, 88
- Watson, C., Povich, M. S., Churchwell, E. B., et al. 2008, ApJ, 681, 1341
- Zavagno, A., Russeil, D., Motte, F., et al. 2010, A&A, 518, L81